Energy-transfer Processes of the Xe ($6p[1/2]_0$, $6p[3/2]_2$, and $6p[5/2]_2$) Atoms under the Condition of Ultrahigh Pumped Power

Shan He,[1,2] Junzhi Chu,[1,2] Dong Liu,[1] Xueyang Li,[1,2] Jingwei Guo,[*,1] Jinbo Liu,[1] Shu Hu,[1] Hui Li,[1] Pengyuan Wang,[1] Ying Chen, [1]Fengting Sang,[1] Yuqi Jin[1]

[1]*Key Laboratory of Chemical Lasers, Dalian Institute of Chemical Physics, Chinese Academy of Sciences, Dalian, 116023, P. R. China*

[2]*University of Chinese Academy of Sciences, Beijing, 100049, P. R. China*

The kinetic processes of the Xe ($6p[1/2]_0$, $6p[3/2]_2$, and $6p[5/2]_2$) Atoms under the focused condition were investigated. The atomic density of the laser prepared state significantly increases. Therefore, the probability of the energy-pooling between two high-lying atoms augments. There are three major types of the energy-pooling collisions. The first type is the energy-pooling ionization. Once the excitation laser is focused, the obvious ionization can be observed from the side window whenever the laser prepared state is $6p[1/2]_0$, $6p[3/2]_2$, or $6p[5/2]_2$ state. Ionization of Xe is attributed to the energy-pooling ionization or a Xe^* atom reabsorbing another excitation photon. The second type is energy-pooling with big energy difference. When the laser prepared state is the $6p[1/2]_0$ state, the energy-pooling collision between the two $6p[1/2]_0$ atoms can produce one $5d[3/2]_1$ atom and one $6s'[1/2]_0$ atom. The third type is energy-pooling with small energy difference. The intensities of the fluorescence lines that the higher states are five secondary 6p states are much stronger and the rising edges of these fluorescence lines are much steeper. The primary mechanism of generating the secondary 6p atoms is energy-pooling collision instead of collision relaxation. Based on the collision probability, the rate of energy-pooling between two $6p[1/2]_0$ atoms is deduced (4.16×10^8 s^{-1}). In addition, the 6s atoms also increase under the focused condition.

Therefore, all the fluorescence lines are serious trailing by radiation trapping.

Key words: Energy-pooling, Kinetics, Xe, Ultrahigh pumped power

I. Introduction

Recently, diode-pumped metastable rare gas laser is a promising subject for its unique advantages including mild working conditions and inert chemical property etc.. So many groups pay their attentions to this subject [1-9]. Heaven and co-workers have demonstrated a CW diode-pumped Ar^* laser providing 4 W [9]. It is a great progress in the regime of diode-pumped rare gas laser.

The study about diode-pumped metastable Xe laser is sparse. In comparison with the lighter rare gas atoms, the metastable Xe atoms are easier to produce. However, the kinetics between the high-lying Xe states is very complex for the energy differences between the high-lying Xe states being relatively low. Some works have studied the energy-transfer processes between the high-lying Xe states [10, 11]. But the power of the excitation laser is relatively low. However, the laser system usually acquires high power pumped sources. Consequently, it is important to study the energy-transfer processes between the high-lying Xe states under the high power pumped condition.

Energy-pooling collisions can be produced in diode-pumped alkali lasers (DPAL) under the strong pumping condition[12]. Energy pooling is a kinetic process in which two excited atoms collide to produce one atom in a higher state and the other one in a lower state. This process has been widely studied in alkali metals [13, 14] and alkaline earth metals [15, 16]. The high-lying states of the rare gas atoms are more abundant. However, studies about energy-pooling collision between the high-lying Xe states are sparse.

Previously, we have studied kinetics of the $6p[1/2]_0$ state under the condition of strong excitation laser. We have found that the high power of the excitation laser can trigger the ASE of

3408 nm ($6p[1/2]_0$−$6s'[1/2]_1$) [17]. We have systematically studied the kinetics of $6p[1/2]_0$ atoms in buffer gases and found that the Kr, Ar, and Ne buffer gases can accelerate the transfers of $6p[1/2]_0 \rightarrow 5d[1/2]_1$[18]. However, the energy-pooling collision has never been observed. Although the power of the excitation laser we used is relatively high, the energy-pooling collision may need even higher power.

In this work, the time-resolved fluorescence and ASE spectra were detected under the focused condition. Only when the excitation laser is resonant and focused, can ionization phenomenon be observed. The ionization should be produced by energy-pooling collision or the high-lying atoms reabsorbing excitation photons. When the laser prepared state is the $6p[1/2]_0$ state, two new ASE lines at 1732 nm ($5d[3/2]_1$-$6p[5/2]_2$) and 2026 nm ($5d[3/2]_1$-$6p[3/2]_1$) appear. The substantial $5d[3/2]_1$ atoms are produced by energy-pooling collision between two $6p[1/2]_0$ atoms. By virtue of the unique arrangements near the $5d[3/2]_1$ and $6s'[1/2]_0$ states, the probability of self-pooling (equation 3) can be pretty high. Besides, all the intensities of fluorescence lines with the higher states being secondary 6p states become stronger, and the rising edges of those lines are much steeper under the focused condition. Therefore, the primary mechanism of producing the secondary 6p atoms should be the energy-pooling collision instead of collision relaxation.

II. Experimental methods

The experimental apparatus has been described in detail previously [17, 18]. Only brief description was given here. The excitation laser was obtained from the second harmonic of dye laser (Sirah CBST−LG−18−EG). The Xe ($6p[1/2]_0$, $6p[3/2]_2$, and $6p[5/2]_2$) atoms were prepared by two-photon excitation at wavelengths about 249.5, 252.4, and 255.9 nm, respectively. The dye laser was pumped by the third harmonic of a Nd:YAG laser (Beamtech SGR−10). A quartz lens (f = 200

mm) was used to focus the excitation laser. A stainless-steel sample cell was used to contain the gases. It has four windows. One window is made of sapphire to ensure the MIR pass through. The rest three windows are made of fused quartz. An uncoated Si plate was placed between the sapphire window of the cell and the slit of the MIR monochromator (HORIBA micro HR MHRA-2A-MS). It can absorb the excitation laser and transmit the MIR ASE.

A series of lenses was placed along the axis perpendicular to the axis of excitation laser to collect the fluorescence. The focal point of the excitation laser and that of the fluorescence collection lens systems nearly overlap. The fluorescence was separated by a monochromator (Princeton Instrument SpectraPro 2500i) with a 1200 g/mm grating. A single spontaneous emission line was measured by an APD and recorded by a 2 GHz oscilloscope (LeCroy waverunner 620zi). The schematic diagram was shown in Fig. 1.

All the gases used in this experiment are ultrahigh purity Xe (99.999%), Kr (99.999%), Ar (99.999%).

III. Results and discussion

Fig. 2 shows the phenomena directly observed from the side window. Evidently, strong visible emissions are produced under the resonant and focused condition. The upper states of these emissions are not the six 6p states. The wavelengths of emissions with the upper states being 6p states are all longer than 800 nm. In addition, there is no visible emission under the resonant and unfocused condition. There must be some new processes happening under the resonant and focused condition. To probe the new process, the fluorescence spectrum was observed under the resonant and focused condition and shown in Fig. 3. Firstly, the typical the fluorescence lines of 6p-6s such as 828 nm($6p[1/2]_0-6s[3/2]_1$), 823 nm ($6p[3/2]_2-6s[3/2]_2$), and 882 nm ($6p[5/2]_3-6s[3/2]_2$) are

observed.

Secondly, the continuous spectrum from 400-700 nm is obviously produced by ionization. The Xe atoms are ionization under the resonant and focused condition and these two factors are both indispensable. The ionization processes should occur as follows (Xe^* is the laser prepared state including the $6p[1/2]_0$, $6p[3/2]_2$, and $6p[5/2]_2$ states):

$$Xe^* + Xe^* \xrightarrow{\text{collision}} Xe_2^+ + e \longrightarrow Xe^+ + Xe + e \quad (1)$$

$$Xe^* + h\gamma \longrightarrow Xe^+ \quad (2)$$

The first mechanism (equation 1) is the "energy-pooling ionization". Substantial Xe^* atoms are generated near the focal point under the resonant and focused condition. It increases the probability of the effective collision between the two Xe^* atoms. Since the potential energy of Xe_2^+ is ~ 90000 cm^{-1} [19], the potential energies of two Xe^* atoms (higher than 154000 cm^{-1}) are high enough to trigger the equation 1. The second mechanism (equation 2) is that a Xe^* atom absorbs another excitation photon. Not only the Xe^* density but also the photon density of excitation laser is very high in the area near the focal point. Thus the probability of equation 2 can also increase. In addition, the potential energy of Xe^* is bigger than 78000 cm^{-1}. The energy of a ~250 nm photon is ~40000 cm^{-1}. The energy sum of a Xe^* and an excitation photon is high enough to trigger the ionization. Because no ionization phenomenon appears under the non-resonant and focused condition, the mechanism of a ground state Xe atom absorbing three or more photons is excluded.

Thirdly, the atomic lines in 450-500 nm can be owed to the lines of 6p'-6s and 7p-6s, such as 450 nm ($6p'[1/2]_0$-$6s[3/2]_2$), 467 nm ($7p[5/2]_3$-$6s[3/2]_2$), 482 nm ($7p[3/2]_1$-$6s[3/2]_1$). The energy differences between the $6p[1/2]_0$ state and 6p', 7p states are ~9000 cm^{-1}. Relaxation normally cannot produce exothermic transfer, let alone the exothermic transfer with such a big energy

difference. The following two mechanisms may explain the production of 6p' and 7p atoms. The first mechanism is a Xe^+ combining an electron to populate a 6p' or 7p atom. The second mechanism is energy-pooling between two 6p atoms.

Fig. 4 is the mid-infrared ASE spectra measured in the forward direction along the excitation laser. The laser prepared state is the $6p[1/2]_0$ state. As shown in the Fig. 4a, the intensity of ASE at 3408 nm ($6p[1/2]_0$−$6s'[1/2]_1$) in pure Xe under the focused condition is much stronger than that under the unfocused condition. The density of the $6p[1/2]_0$ atoms significantly increases in the region near the focal point. It results in the high gain coefficient of the ASE at 3408 nm ($6p[1/2]_0$−$6s'[1/2]_1$). So the intensity of ASE at 3408 nm ($6p[1/2]_0$−$6s'[1/2]_1$) becomes stronger. Unexpectedly, new peaks at 1732 nm, 2026 nm, 3464 nm, and 4052 nm emerge. The peaks at 1732 nm and 2026 nm should be attributed to the transfers of $5d[3/2]_1$-$6p[5/2]_2$ and $5d[3/2]_1$-$6p[3/2]_1$, respectively. And the peaks at 3464 nm and 4052 nm are the second order diffraction of the peaks at 1732 nm and 2026 nm, respectively. This phenomenon indicates substantial $5d[3/2]_1$ atoms are produced. The kinetic process for the generation of $5d[3/2]_1$ atoms should be energy-pooling collision illustrated as equation 3. The probability of equation 3 must be pretty high, because the population inversions can be formed between the $5d[3/2]_1$ state and the $6p[5/2]_2$, $6p[3/2]_1$ states. This can be owed to the following two aspects. Firstly, the energy difference between the $6p[1/2]_0$ state and the $5d[3/2]_1$ state is very close to that between the $6p[1/2]_0$ state and the $6s'[1/2]_0$ state. To some extent, this energy-pooling collision is a near−resonance process. Secondly, the energy level arrangements near the $5d[3/2]_1$ state and the $6s'[1/2]_0$ state are unique. As shown in Fig. 5, both of these two states have big energy differences to the adjacent states (E ($7s[3/2]_2$) – E ($5d[3/2]_1$) = 1298.8 cm^{-1}, E ($5d[3/2]_1$) – E ($5d[5/2]_3$) = 1459.8 cm^{-1}, E ($6s'[1/2]_1$) – E ($6s'[1/2]_0$) = 988.2 cm^{-1}, E

(6s'[1/2]$_0$) – E (6s[3/2]$_1$) = 8151.6 cm^{-1}). Once one 6p[1/2]$_0$ atom reaches the 6s'[1/2]$_1$ state, another 6p[1/2]$_0$ atom strongly tends to reach the 5d[3/2]$_1$ state.

$$\mathrm{Xe(6p[1/2]_0) + Xe\left(6p[1/2]_0\right) \xrightarrow{\text{collision}} Xe(6s'[1/2]_0) + Xe(5d[3/2]_1) + \Delta E} \quad (3)$$
$$\Delta E = -151.18\mathrm{cm}^{-1}$$

Ar and Kr atoms can accelerate the transfer of 6p[1/2]$_0$→5d[1/2]$_1$[10, 11, 18]. Therefore, they can switch ASE channel from 3408 nm (6p[1/2]$_0$−6s'[1/2]$_1$) to 3680 nm (5d[1/2]$_1$−6p[1/2]$_1$) by collision[18]. Accordingly, ASE spectra in buffer gas of Ar or Kr have two peaks at 3408 nm and 3680 nm are shown in the Fig. 4b and 4c. The intensity of ASE at 3680 nm decreases and new peaks at 1732 nm, 2026 nm, 3464 nm, and 4052 nm emerge under the focused condition. The probability of collision between one 6p[1/2]$_0$ atom and another atom is described as equation 4.

$$z = \pi d_{AB}^2 \sqrt{\frac{8RT}{\pi\mu}} n_A n_B \quad (4)$$

Where z is the collision probability between A and B, d_{AB} is the sum of radius of A and B, μ is the reduced mass of A and B, T is the temperature, n_A and n_B are the concentration of A and B, respectively.

Obviously, collision probability between A and B is proportional to the concentration of buffer atoms. Although the density of the 6p[1/2]$_0$ atoms near the focal point is high, it must be much lower than the density of Ar or Kr atoms (D_{Rg} = ~2.57 × 10^{17} cm^{-3}). Consequently, the probability of collision between two 6p[1/2]$_0$ atoms is much lower than that between one 6p[1/2]$_0$ atom and one buffer gas atom. However, Fig. 4b and 4c reflect that the primary kinetic process under the focused condition is the energy-pooling collision instead of collision relaxation. It indicates that the collision between two 6p[1/2]$_0$ atoms is more effective than that between a 6p[1/2]$_0$ atom and a buffer gas atom (Ar or Kr), because 6p[1/2]$_0$ atoms are more active than ground state Ar and Kr atoms.

Based on the analysis above, if the density of $6p[1/2]_0$ atoms holds constant, the rate of energy pooling is constant. Some semi-quantitative deductions are given here. The pressure of Xe and excitation power hold constant. We suppose that the rate of energy-pooling is V. Then the Ar is filled into the cell. The probability of collision between Xe* and Ar is increase. The rate of relaxation can be expressed as $k^{Ar}_{6p[1/2]_0,T} \times p$. Ar can switch the ASE channel from 3408 nm ($6p[1/2]_0-6s'[1/2]_1$) to 3680 nm ($5d[1/2]_1-6p[1/2]_1$). It is attributed to the high value of $k^{Ar}_{6p[1/2]_0,5d[1/2]_1}$. With the increasing pressure of Ar, the ASE at 3680 nm should gradually increase, the ASE at 3408 nm and 1732 nm should gradually decrease. As shown in Fig. 6, the actual phenomenon precisely follows this prediction. Then the intensity of 3680 nm is proportional to $\frac{k^{Ar}_{6p[1/2]_0,5d[1/2]_1} \times p}{V + k^{Ar}_{6p[1/2]_0,T} \times p}$ as equation 5. Then we can introduce a parameter "α" to modify the intensity of 3680 nm. Equation 5 can be rewritten as equation 6. According to this equation, $\frac{1}{I_{3680}}$ should be linear with $\frac{1}{p}$ as equation 7. Then the slope $\frac{\alpha \times V}{k^{Ar}_{6p[1/2]_0,5d[1/2]_1}}$ and intercept $\frac{\alpha \times k^{Ar}_{6p[1/2]_0,T}}{k^{Ar}_{6p[1/2]_0,5d[1/2]_1}}$ can be deduced. The value of $k^{Ar}_{6p[1/2]_0,T}$ and $k^{Ar}_{6p[1/2]_0,5d[1/2]_1}$ have been deduced in our previous work.[18] Then the parameter "α" can be deduced. The values of "α", $k^{Ar}_{6p[1/2]_0,5d[1/2]_1}$, and $\frac{a \times V}{k^{Ar}_{6p[1/2]_0,5d[1/2]_1}}$ are all known. As a result, V = 6.39 $\times 10^8$ s^{-1}.

$$I_{3680} \propto \frac{k^{Ar}_{6p[1/2]_0,5d[1/2]_1} \times p}{V + k^{Ar}_{6p[1/2]_0,T} \times p} \quad (5)$$

$$\alpha \times I_{3680} = \frac{k^{Ar}_{6p[1/2]_0,5d[1/2]_1} \times p}{V + k^{Ar}_{6p[1/2]_0,T} \times p} \quad (6)$$

$$\frac{1}{I_{3680}} = \frac{\alpha \times V}{k^{Ar}_{6p[1/2]_0,5d[1/2]_1} \times p} + \frac{\alpha \times k^{Ar}_{6p[1/2]_0,T}}{k^{Ar}_{6p[1/2]_0,5d[1/2]_1}} \quad (7)$$

When the laser prepared state is the $6p[1/2]_0$ state, the time-resolved fluorescence lines of 6p-6s were shown in Fig. 8. The intensity of 828 nm under the focused condition is much stronger than that under the unfocused condition. It results from the high density of the $6p[1/2]_0$ atom under the focused condition. The rest five fluorescence lines can reflect the populations of the five secondary 6p states. Under the unfocused condition, the primary mechanism generating the $6p[3/2]_2$, $6p[3/2]_1$, $6p[5/2]_3$, and $6p[5/2]_2$ atoms is collisional relaxation. The intensities of these fluorescence lines are weak. Obviously, the intensities of fluorescence lines of 823 nm, 916 nm, 882 nm, and 904 nm are much stronger and their rising edges are much steeper under the focused condition. Therefore, a new mechanism, energy-pooling collision, should emerge under the focused condition described as equation 8. Collision of this type between the two $6p[1/2]_0$ atoms can lead to one atom reaching a higher state and the other one reaching a lower state. Besides, the ASE at 1732 nm ($5d[3/2]_1$-$6p[5/2]_2$) and 2026 nm ($5d[3/2]_1$-$6p[3/2]_1$) can also populate the $6p[5/2]_2$ state and the $6p[3/2]_1$ state, respectively. This is another reason why the intensities of 916 nm and 904 nm become stronger. The dominant mechanism of populating $6p[1/2]_1$ atoms is a series of processes related to the ASE at 3408 nm ($6p[1/2]_0$−$6s'[1/2]_1$) and 3680 nm ($5d[1/2]_1$−$6p[1/2]_1$) under the unfocused condition[17, 18]. According to Fig. 4, the intensity of ASE at 3408 nm increases and that at 3680 nm decreases under the focused condition. Thus the population of the $6p[1/2]_1$ atoms should be mainly owed to the processes related to the ASE at 3408 nm. Another phenomenon shown in the Fig. 8 is that all the fluorescence lines are serious trailing under the focused condition. The lifetimes of these states are ~30 ns [10, 11, 17]. However, even at ~1500 ns, all these fluorescence lines are still observed. It means that there still exist some channels populating these 6p atoms even at ~1500 ns. Maybe the channel populating these 6p atoms is radiation trapping. This

phenomenon was widely reported in high-lying states of alkali metals [20] and some states of rare gases [21]. The mechanism of this phenomenon is that radiation near a resonance line can be absorbed and emitted many times before escaping. Then, the apparent radiative lifetime of the higher state can be obviously extended by this effect. However, the prerequisite of radiation trapping is that the population density of the lower state is high enough. If the population density of the lower state is relatively low, the radiation cannot be effectively absorbed. Then, the radiation cannot be trapped by absorbing and emitting many times. The lifetimes of alkali metal states and 6s states of Xe are usually affected by this effect[20, 21], since the lower state is the ground state. However, the 6p states of Xe hardly ever be affected for the lower state being the 6s state. The situation may be different in our work. Not only the density of the $6p[1/2]_0$ state but also those of the 6s states should be very high in the area near the focal point. Then the radiation lines with the higher states being the 6p states can be trapped. The trailing of the fluorescence line is probably due to this reason.

$$Xe(6p[1/2]_0) + Xe\left(6p[1/2]_0\right) \xrightarrow{\text{collision}} Xe(6p) + Xe(5d) \quad (8)$$

When the laser prepared state is the $6p[3/2]_2$ state, Time-resolved fluorescence lines of 6p-6s under both the focused and unfocused conditions were shown in Fig. 9. Under the unfocused condition, the fluorescence lines of 916 nm, 882 nm, 904 nm, and 980 nm were observed, while that of 828 nm could not be observed. It indicates that the $6p[3/2]_2$ atoms can reach the lower states including the $6p[3/2]_1$, $6p[5/2]_3$, $6p[5/2]_2$, and the $6p[1/2]_1$ state but cannot reach the higher state ($6p[1/2]_0$). Collision relaxation usually cannot cause endothermic transfer with big energy difference. However, under the focused condition, the fluorescence at 828 nm was observed. The

$6p[1/2]_0$ atoms cannot be produced by collision relaxation. The mechanism is probably an energy-pooling process between two $6p[3/2]_2$ atoms. Besides, intensities of all the fluorescence lines are much stronger and the rising edges of all the fluorescence lines are much steeper under the focused condition. It should be also owed to the energy-pooling collision. Similar to the phenomenon shown in Fig. 8, the fluorescence lines are serious trailing under the focused condition. The reason is attributed to the radiation trapping. When the laser prepared state is the $6p[5/2]_2$ state, Time-resolved fluorescence lines of 6p-6s under the focused and unfocused conditions were shown in Fig. 10. The phenomena are similar to those shown in Fig. 9. The collision relaxation can cause the endothermic transfer of $6p[5/2]_2 \rightarrow 6p[5/2]_3$ for small energy difference, but the endothermic transfers for big energy differences are hard to generate by collision relaxation. Therefore, the primary mechanism for producing the $6p[1/2]_0$, $6p[3/2]_2$, $6p[3/2]_1$, and $6p[5/2]_3$ atoms is the energy-pooling collision instead of collision relaxation under the focused condition. And the serious trailing is probably owed to the radiation trapping.

IV. Conclusion

The kinetic processes of Xe atoms in the $6p[1/2]_0$, $6p[3/2]_2$, and $6p[5/2]_2$ states were studied under the focused condition. The density of the atoms in the laser prepared state under the focused condition is much higher than that under the unfocused condition. The atoms in the high-lying state are much more active than the atoms in the ground state. Then, the collision between two $6p[1/2]_0$ atoms is more effective than that between a $6p[1/2]_0$ atom and a buffer gas atom (Ar or Kr). Therefore, primary mechanism is the energy-pooling collision instead of the collision relaxation under the focused condition. Since the Xe states are more complex than alkali metals states, the energy-pooling collisions are more abundant among high-lying Xe atoms.

The phenomenon observed from the side window is the energy-pooling ionization. The energies of these three laser prepared states are all high enough to trigger the ionization. When the laser prepared state is the $6p[1/2]_0$ state, two new ASE peaks at 1732 nm ($5d[3/2]_1$-$6p[5/2]_2$) and 2026 nm ($5d[3/2]_1$-$6p[3/2]_1$) appear. Thanks to the unique energy level arrangements near the $5d[3/2]_1$ state and the $6s'[1/2]_0$ state, two $6p[1/2]_0$ atoms strongly tend to pool their internal energy to produce one $5d[3/2]_1$ atom and one $6s'[1/2]_0$ atom. Based on the collision probability, the rate of energy-pooling between two $6p[1/2]_0$ atoms is deduced (4.16×10^8 s^{-1}). The intensities of the all the fluorescence curves increase and their rising edges are steeper under the focused condition. The atoms in the secondary states are mainly produced by energy-pooling collision. Another phenomenon is that even at ~1500 ns, all these fluorescence lines are still observed, although the lifetimes of these states are ~30 ns. The densities of the 6s states should be very high in the area near the focal point. Radiation near a resonance line can be absorbed and emitted many times before escaping. Then the apparent radiative lifetime of the higher state can be obviously extended. The mechanism is probably due to the radiation trapping.

Author information

Corresponding Author

*Jingwei Guo. E−mail: jingweiguo@dicp.ac.cn.

Acknowledgments

This work is supported by the National Natural Science Foundation of China (Grant Nos. 11475177, 61505210) and Key Laboratory of Chemical Laser Foundation (KLCL 2017).

References

[1] M. H. Kabir and M. C. Heaven, J. Phys. Chem. A **115,** 9724 (2011).

[2] J. Han and M. C. Heaven, Opt. Lett. **37,** 2157 (2012).

[3] J. Han, L. Glebov, G. Venus, and M. C. Heaven, Opt. Lett. **38,** 5458 (2013).

[4] J. Han and M. C. Heaven, Opt. Lett. **39,** 6541 (2014).

[5] J. Han and M. C. Heaven, Opt. Lett. **40,** 1310 (2015).

[6] W. T. Rawlins, K. L. Galbally-Kinney, S. J. Davis, A. R. Hoskinson, J. A. Hopwood, and M. C. Heaven, Opt. Express **23,** 4804 (2015).

[7] Z. Yang, G. Yu, H. Wang, Q. Lu, and X. Xu, Opt. Express **23,** 13823 (2015).

[8] P. A. Mikheyev Quantum Electron. **48,** 704 (2015).

[9] J. Han, M. C. Heaven, P. J. Moran, G. A. Pitz, E. M. Guild, C. R. Sanderson, and B. Hokr, Opt. Lett. **42,** 4627 (2017).

[10] J. K. Ku and D. W. Setser, J. Chem. Phys. **84,** 4304 (1986).

[11] J. Xu and D. W. Setser, J. Chem. Phys. **94,** 4243 (1991).

[12] G. An, Y. Wang, J. Han, H. Cai, J. Zhou, W. Zhang, L. Xue, H. Wang, M. Gao, and Z. Jiang, Opt. Express **23,** 26414 (2015).

[13] Z. J. Jabbour, R. K. Namiotka, J. Huennekens, M. Allegrini, S. Milosevic, and F. de Tomasi, Phys. Rev. A **54,** 1372 (1996).

[14] C. Gabbanini, S. Gozzini, G. Squadrito, M. Allegrini, and L. Moi, Phys. Rev. A **39,** 6148 (1989).

[15] W. H. Breckenridge, W. L. Nikolai, and J. Stewart, J. Chem. Phys. **74,** 2073 (1981).

[16] J. F. Kelly, M. Harris, and A. Gallagher, Phys. Rev. A **38,** 1225, (1988).

[17] S. He, Y. Guan, D. Liu, X. Xia, B. Gai, S. Hu, J. Guo, F. Sang, and Y. Jin, J. Phys. Chem. A **121,** 3430 (2017).

[18] S. He, D. Liu, X. Li, J. Chu, J. Guo, J. Liu, S. Hu, F. Sang, and Y. Jin, J. Phys. Chem. A **122,** 5361 (2018).

[19] T. O. Nelson, D. W. Setser, and M. K. Richmann, J. Phys. Chem. **99,** 7482 (1995).

[20] K. C. Brown and G. P. Perram, Phys. Rev. A **85,** 022713−1 (2012).

[21] N. Sadeghi and J. Sabbagh, Phys. Rev. A **16,** 2336 (1977)

Figure Captions

FIG. 1. Schematic diagram of the experimental apparatus.

FIG. 2 The phenomenon directly observed from the side window. The experimental conditions from top to bottom are resonant and unfocused, non-resonant and focused, and resonant and focused, respectively. The excitation state is $6p[1/2]_0$, $6p[3/2]_2$, or $6p[5/2]_2$. The pressure of Xe is 6.0 Torr. The energy of excitation laser is 2.30 mJ (3.54×10^{10} W/cm^2).

FIG 3. Fluorescence spectrum under the resonant and focused condition. The laser prepared state is the $6p[1/2]_0$ state. The pressure of Xe is 6.0 Torr. The energy of excitation laser is 2.30 mJ (3.54×10^{10} W/cm^2).

FIG. 4 The mid-infrared ASE spectra in the forward direction along the excitation laser. The laser prepared state is the $6p[1/2]_0$ state. The energy of excitation laser is 2.30 mJ (3.54×10^{10} W/cm^2). For clear comparison, the spectrum under the focused condition is moved upward 0.50 a.u..

FIG. 5 Schematic diagram of the energy levels of Xe* related to this work. Each state is marked with its energy (in cm^{-1}) in reference to the ground state s_0.

FIG. 6. Plot of ASE at 1732 nm (a), 3408 nm (b), and 3680 nm (c) against pressures of Ar. The pressure of Xe is 6.0 Torr. The energy of excitation laser is 2.30 mJ (3.54×10^{10} W/cm^2).

FIG 7. Plot of $1/I_{3680\ nm}$ against 1/p. The pressure of Xe is 6.0 Torr. The buffer gas is Ar. The energy of excitation laser is 2.30 mJ (3.54×10^{10} W/cm^2). The red line is the result of linear fitting.

FIG. 8 Time-resolved fluorescence lines of the six 6p states under the focused and unfocused conditions. The laser prepared state is the $6p[1/2]_0$ state. The gases contain 6.0 Torr Xe and 8.7 Torr Ar. The energy of excitation laser is 2.30 mJ (3.54×10^{10} W/cm^2). Note: 828 nm ($6p[1/2]_0$-$6s[3/2]_1$),

823 nm ($6p[3/2]_2-6s[3/2]_2$), 916 nm ($6p[3/2]_1-6s[3/2]_1$), 882 nm ($6p[5/2]_3-6s[3/2]_2$), 904 nm ($6p[5/2]_2-6s[3/2]_2$), and 980 nm ($6p[1/2]_1-6s[3/2]_2$).

FIG. 9 Time-resolved fluorescence lines of the six 6p states under the focused and unfocused conditions. The laser prepared state is the $6p[3/2]_2$ state. These plots were obtained in pure Xe. And the pressure of Xe is 6.0 Torr. The energy of excitation laser is 2.30 mJ (3.54×10^{10} W/cm^2).

FIG. 10 Time-resolved fluorescence lines of the six 6p states under the focused and unfocused conditions. The laser prepared state is the $6p[5/2]_2$ state. These plots were obtained in pure Xe. And the pressure of Xe is 6.0 Torr. The energy of excitation laser is 1.50 mJ (2.31×10^{10} W/cm^2).

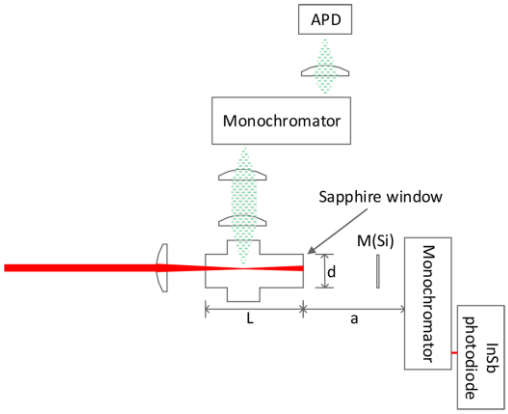

FIG. 1 Schematic diagram of the experimental apparatus.

FIG. 2 The phenomenon directly observed from the side window. The experimental conditions from top to bottom are resonant and unfocused, non-resonant and focused, and resonant and focused, respectively. The excitation state is $6p[1/2]_0$, $6p[3/2]_2$, or $6p[5/2]_2$. The pressure of Xe is 6.0 Torr. The energy of excitation laser is 2.30 mJ (3.54×10^{10} W/cm^2).

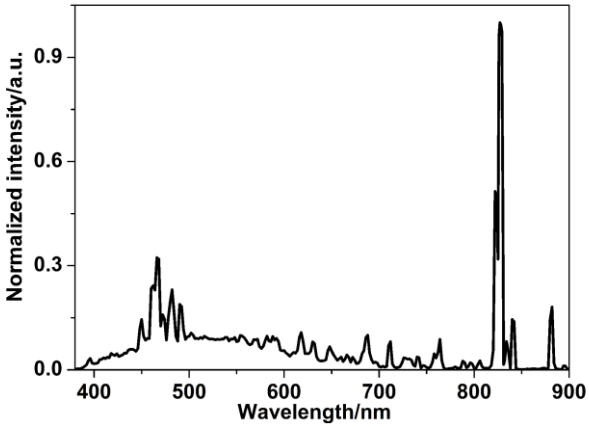

FIG 3. Fluorescence spectrum under the resonant and focused condition. The laser prepared state is the $6p[1/2]_0$ state. The pressure of Xe is 6.0 Torr. The energy of excitation laser is 2.30 mJ (3.54×10^{10} W/cm^2).

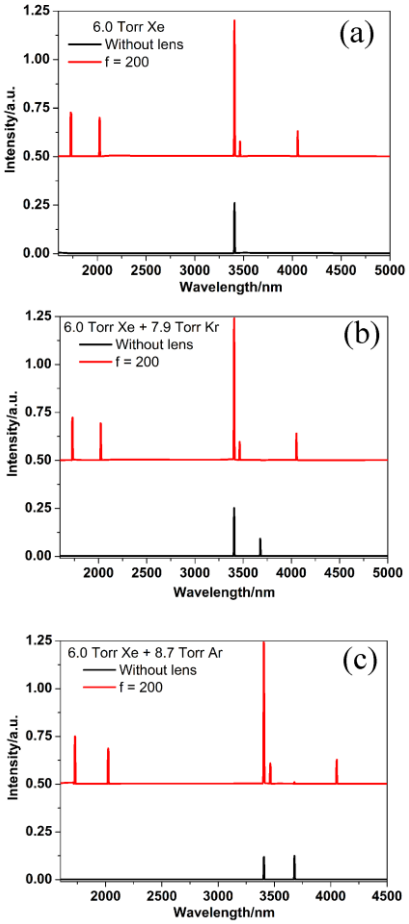

FIG. 4 The mid-infrared ASE spectra in the forward direction along the excitation laser. The laser prepared state is the $6p[1/2]_0$ state. The energy of excitation laser is 2.30 mJ (3.54×10^{10} W/cm^2). For clear comparison, the spectrum under the focused condition is moved upward 0.50 a.u..

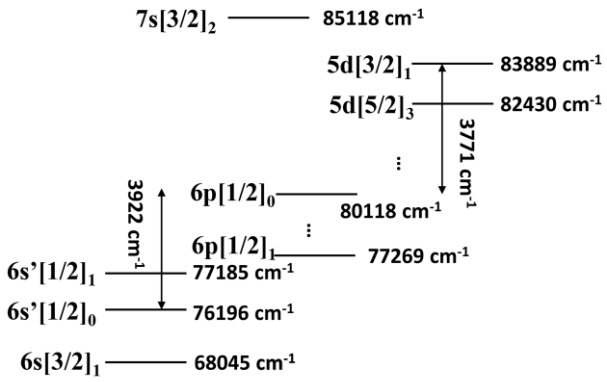

FIG. 5 Schematic diagram of the energy levels of Xe* related to this work. Each state is marked with its energy (in cm^{-1}) in reference to the ground state s_0.

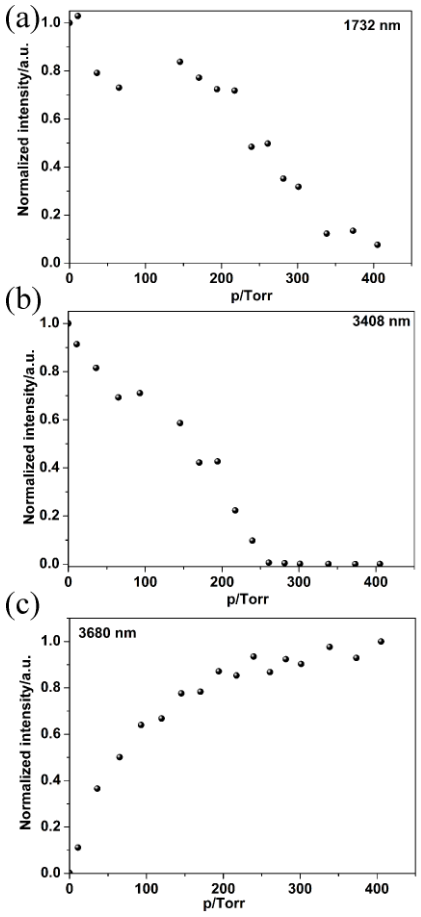

FIG. 6. Plot of ASE at 1732 nm (a), 3408 nm (b), and 3680 nm (c) against pressures of Ar. The pressure of Xe is 6.0 Torr. The energy of excitation laser is 2.30 mJ (3.54×10^{10} W/cm^2).

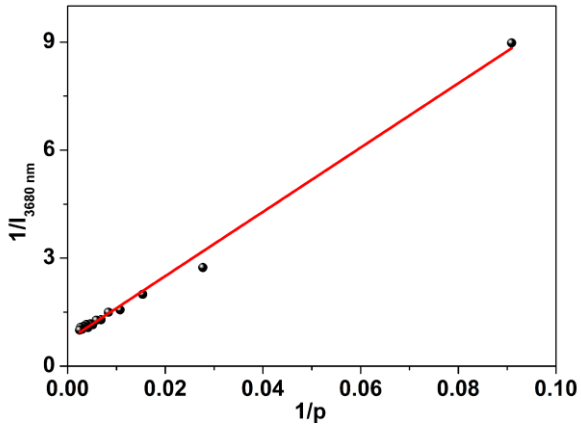

FIG 7. Plot of $1/I_{3680\ nm}$ against 1/p. The pressure of Xe is 6.0 Torr. The buffer gas is Ar. The energy of excitation laser is 2.30 mJ (3.54×10^{10} W/cm^2). The red line is the result of linear fitting.

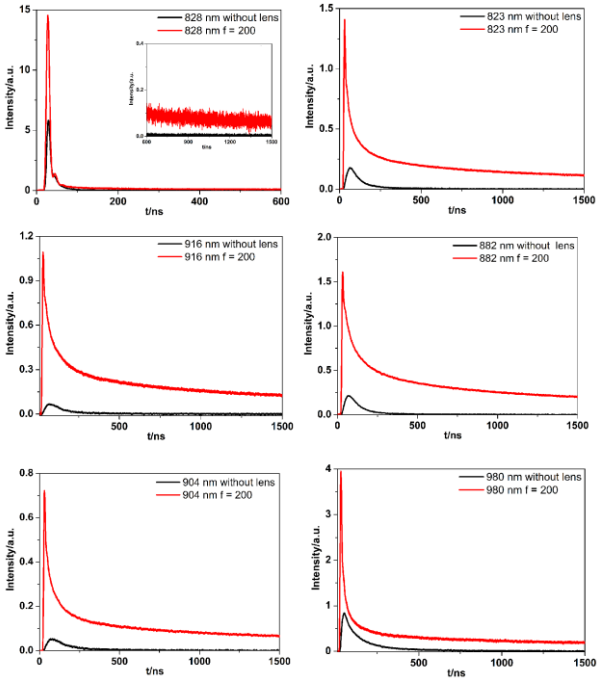

FIG. 8 Time-resolved fluorescence lines of the six 6p states under the focused and unfocused conditions. The laser prepared state is the $6p[1/2]_0$ state. The gases contain 6.0 Torr Xe and 8.7 Torr Ar. The energy of excitation laser is 2.30 mJ (3.54×10^{10} W/cm^2). Note: 828 nm ($6p[1/2]_0$-$6s[3/2]_1$), 823 nm ($6p[3/2]_2$−$6s[3/2]_2$), 916 nm ($6p[3/2]_1$−$6s[3/2]_1$), 882 nm ($6p[5/2]_3$−$6s[3/2]_2$), 904 nm ($6p[5/2]_2$−$6s[3/2]_2$), and 980 nm ($6p[1/2]_1$−$6s[3/2]_2$).

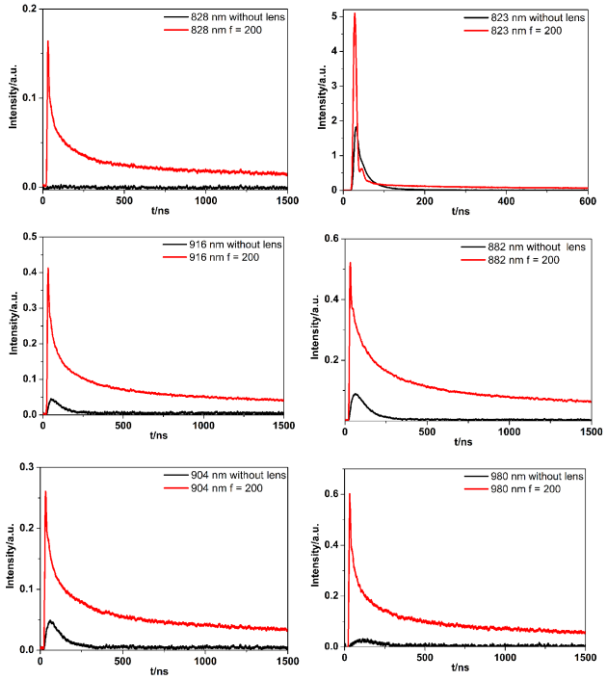

FIG. 9 Time-resolved fluorescence lines of the six 6p states under the focused and unfocused conditions. The laser prepared state is the $6p[3/2]_2$ state. These plots were obtained in pure Xe. And the pressure of Xe is 6.0 Torr. The energy of excitation laser is 2.30 mJ (3.54×10^{10} W/cm^2).

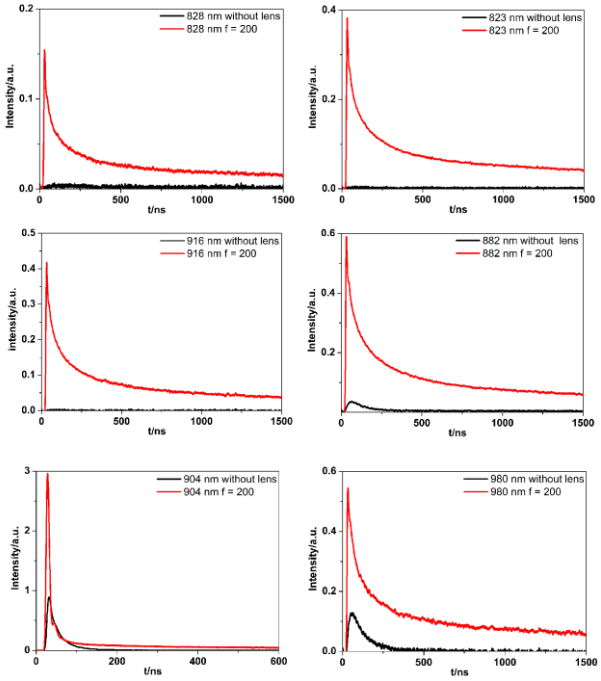

FIG. 10 Time-resolved fluorescence lines of the six 6p states under the focused and unfocused conditions. The laser prepared state is the $6p[5/2]_2$ state. These plots were obtained in pure Xe. And the pressure of Xe is 6.0 Torr. The energy of excitation laser is 1.50 mJ (2.31×10^{10} W/cm^2).